Selectivity modulation during electrochemical reduction of nitrate by electrolyte engineering

Ana Sofia Fajardo, Paul Westerhoff, Sergi Garcia-Segura, Carlos M Sánchez-Sánchez

Selectivity modulation during electrochemical reduction of nitrate by electrolyte engineering

Ana S. Fajardo[a,b,*], Paul Westerhoff[b], Sergi Garcia-Segura[b] and Carlos M. Sánchez-Sánchez[a,**]

[a]Sorbonne Université, CNRS, Laboratoire Interfaces et Systèmes Electrochimiques (LISE), 4 place Jussieu, F-75005, Paris, France

[b]Nanosystems Engineering Research Center for Nanotechnology-Enabled Water Treatment, School of Sustainable Engineering and the Built Environment, Arizona State University, Tempe, AZ 85287-3005, USA

Corresponding author:

*e-mail: sofia.fajardo@ipc.pt (Dr. Ana Sofia Fajardo)

**e-mail: carlos.sanchez@sorbonne-universite.fr (Dr. Carlos M. Sanchez-Sanchez)

Abstract

This article explores how electrolyte engineering can control product selectivity and kinetics of electrochemical reduction of nitrate (ERN). This is an alternative approach to the conventional catalyst engineering methodology for controlling the electrode/electrolyte interface and impact on ERN activity and selectivity. Electrolytic treatment was conducted in a membrane-less plug flow reactor (PFR) under batch recirculation using a tin cathode. Operational parameters related to solution flow rate, mass transport regime, initial pH, and dissolved oxygen demonstrated to have negligible impact on nitrate (NO_3^-) removal under the operation conditions studied. In stark contrast, the presence of different alkali cations in solution (Li^+, Na^+, K^+ and Cs^+) sharply impacted on NO_3^- removal rate and steered product selectivity in ERN, as well as they did it for the case of nitrite (NO_2^-) reduction reaction. An evident increase in ammonia (NH_3) production is achieved in both NO_3^- and NO_2^- removal by following the order $Li^+ < Na^+ \approx K^+ < Cs^+$. These close tendencies observed for NO_3^- and NO_2^- reduction reactions point out the electrostatic effect stabilizing negatively charged species at the electrode interface as the main responsible of selectivity modulation through electrolyte engineering. Thus, we present the first evidence of a significant shift in products selectivity in ERN from N_{gas} towards NH_3 production on tin electrodes by tuning the electrode-electrolyte interface with suitable cations. Furthermore, an approximately 2-fold decrease in electrical energy per order is achieved by solutions containing Cs^+ instead of Li^+ for both NO_3^- and NO_2^- reduction reactions. These results open the pathway towards understanding interfacial impacts associated to different ionic species present in solution that can enhance electrochemical pollutants removal, and resource recovery, as well as lowering the process cost.

Keywords: Nitrate/nitrite-nitrogen pollution; Electrochemical water treatment; Tin electrode material; Product selectivity; Alkali cation

1. Introduction

Nitrate (NO_3^-) is considered one of the ten most frequently reported drinking water quality violations worldwide and commonly found at concentrations above the maximum contaminant level (MCL > 10 mg NO_3^--N L^{-1}) [1,2]. During the last century, due to the anthropogenic nitrogen fertilizer inputs, NO_3^- concentrations in surface and ground waters have dramatically increased [3]. Exposure to NO_3^- levels above MCL in drinking water may lead to serious health risks in humans such as respiratory problems and cancer [4–7]. To overcome this challenge that affects ca. 45 million people in the US [2,8], different water treatment processes based on biological and physical methodologies have been applied to remove NO_3^- from aquatic streams. However, the requirement of large facilities and post-treatment of waste generated from those technologies became a major drawback for small water systems at household level for people that rely on unmonitored wells [9–13]. For this reason, decentralized NO_3^- polluted water treatment by electrocatalytic processes represents an emerging and sustainable alternative technology to conventional methods [14].

A significant percentage of the electrochemical reduction of nitrate (ERN)-related literature corresponds to the study of electrode materials that can selectively reduce NO_3^- to innocuous nitrogen gas (N_2) [15–20] Additionally, ERN has recently gained attention for the green production of an interesting added value product: ammonium ion (NH_4^+) or ammonia (NH_3) contributing to advance circular economy strategies and at the same time decreasing the high costs associated to the Haber-Bosh process [21,22]. The electrochemical process may therefore promote a sustainable decentralized ammonia recovery where enriched water for crops irrigation can be a potential application for this added value product [23]. So far, the electrocatalyst tailored design has been the preferred methodology for controlling the electrode/electrolyte interface and impact on ERN. This is mainly focused on varying the electrode material composition through crystallographic plane control [24,25], alloys [26,27], nanocomposite engineering [28,29], or single-atom control [30,31]. Lately, Cu-Co-based materials concentrate a lot of attention for enhancing ammonia production [32–37]. However, little attention has been paid to the effect that the electrolyte, and particularly the cations, may have on the ERN activity and selectivity control, as well as on

the process cost. The electrolyte/electrode interface is where electrochemical reactions take place. Thus, modulating the interfacial phenomena by varying the cation electrolyte might affect the local electric field, the interfacial pH and/or the stabilization of reaction intermediates during the electrochemical reaction [38]. A few attempts to study the nature of the supporting electrolyte on ERN were reported [39,40]. But, to the best of our knowledge, this is the first time that the study of electrolyte composition is applied to both NO_3^- and nitrite (NO_2^-) reduction reactions using a batch recirculating plug flow reactor (PFR) under galvanostatic conditions, which represent feasible conditions in large-scale applications.

This manuscript studies a broad variety of alkali cations (Li^+, Na^+, K^+ and Cs^+) in solution for exploring the shift in selectivity from N_2 to NH_3 production during ERN on a Sn cathode, which is a well-established active catalyst for N_2 and poor catalyst for NH_3 production [15,41,42]. This represents a proof of concept for the electrolyte engineering strategy applied to water pollutants remediation, which is based on tuning the electrode/electrolyte interfacial electric field [43–46] and represents a powerful and low-cost alternative to alloying or modifying the morphology of the electrode material in electrocatalytic reactions. Moreover, fundamental understanding on how electrolyte composition may steer selectivity and kinetics is essential, since electrocatalysts are generally evaluated in ultrapure solutions containing only NO_3^-. Thus, NO_3^- and NO_2^- reduction rates and products selectivity are reported here together with engineering figures of merit, such as electrical energy per order (EE/O). Herein, it is demonstrated that the preferential selectivity of Sn for N_2 evolution can be shifted towards NH_3 production at low NO_3^- concentration in an alkaline solution by controlling the nature of the cation present in the electrode-electrolyte interface.

2. Materials and methods

2.1 Chemicals

The following chemicals, purchased from Sigma-Aldrich, were used to prepare solutions using ultrapure water with resistivity >18.2 MΩ cm at 25 °C (Elga Purelab Flex, Veolia Water Technologies): sodium nitrate ($NaNO_3$, ≥ 99.0%), sodium nitrite ($NaNO_2$, ≥ 99.0%), ammonium sulfate ($(NH_4)_2SO_4$, 99.5%), cesium hydroxide (CsOH, 99.95%), lithium hydroxide (LiOH, 98.0%), potassium hydroxide (KOH, >

85.0%), sodium hydroxide (NaOH, 99.2%) and sulfamic (amidosulfonic) acid (H_2NSO_3H, ≥ 99%). These reagents were of analytical grade and were used without further purification.

2.2 Electrolysis set-up and operation

Electrocatalytic reductions were carried out in a commercially available batch recirculating membrane-less plug flow reactor (PFR) from ElectroCell Europe A/S. The scheme of the reactor configuration is illustrated in Figure 1. The reactor contains a mass transfer promoter between the electrodes. The ERN electrolysis setup treats 200 mL of a single solution under recirculation at 25 °C testing different flow rates (4.2, 21, and 105 mL min^{-1}) with a peristaltic pump (MasterFlex L/S). All experiments were operated under galvanostatic conditions at 20 mA cm^{-2} for 180 min using a power supply TENMA 72-2720 DC. Commercial tin (Sn – 99.99%, Alfa Aesar) and a Ti/IrO_2 dimensional stable anode (from ElectroCell Europe A/S) plates were used as cathode and anode materials, respectively. The Sn plate active area is considered equivalent to its geometrical surface area (10 cm^2). The interelectrode gap distance between cathode and anode is 4.0 mm. To guarantee a similar and homogeneous initial texture, the surface of the tin cathode was polished with sandpaper (P400 and P1200 grit) before each new electrolysis.

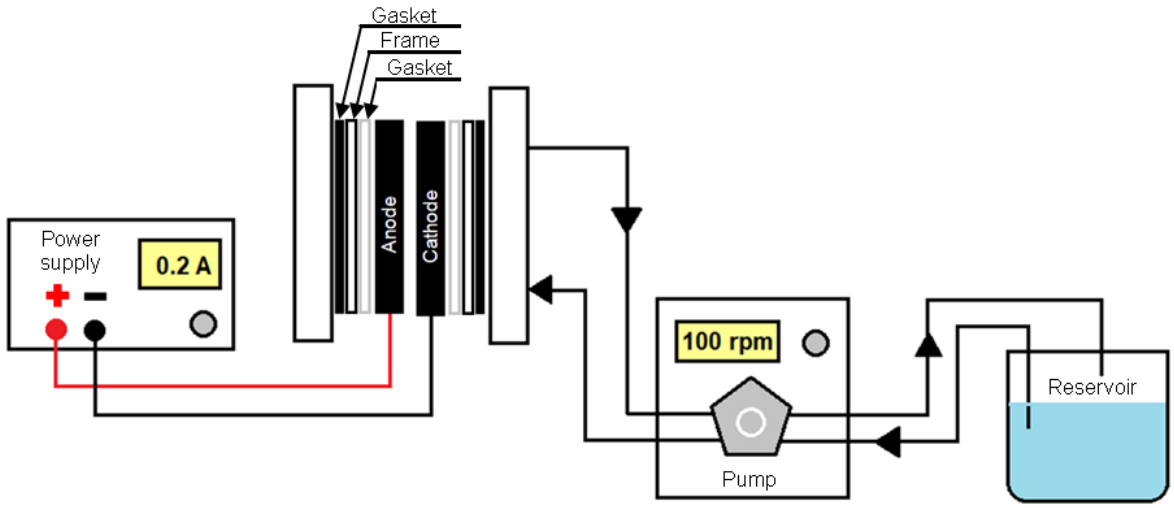

Figure 1. Set-up of the electrochemical reduction system.

To study the electrochemical reduction of NO_3^- and NO_2^-, different solution compositions were prepared:

(i) 100 mg L^{-1} NO_3^--N (from $NaNO_3$) and 50 mM Na_2SO_4 at neutral initial pH (5.85 ± 0.21).

(ii) 100 mg L^{-1} NO_3^--N (from $NaNO_3$), 50 mM Na_2SO_4 and 0.01 mol L^{-1} NaOH at pH (12.03 ± 0.25).

(iii) 100 mg L^{-1} NO_3^--N (from $NaNO_3$), 50 mM Na_2SO_4 and 0.01 mol L^{-1} NaOH at pH (12.03 ± 0.25) deareated solution (Ar bubbling).

(iv) 20 mg L^{-1} NO_3^--N (from $NaNO_3$) and 0.02 mol L^{-1} of electrolyte (CsOH, LiOH, KOH or NaOH) at alkaline pH (12.03 ± 0.25).

(v) 20 mg L^{-1} NO_2^--N (from $NaNO_2$) and 0.02 mol L^{-1} of electrolyte (CsOH, LiOH, KOH or NaOH) at alkaline pH (12.03 ± 0.25).

Most of the NO_3^--contaminated natural treated effluents correspond to unbuffered solutions at neutral pH such as solution (*i*) [47–50]. However, ERN at the cathode provokes the progressive alkalinization of the solution during the electrolysis, reaching very rapidly a stabilized value of the solution pH in the range 11-12 [15] (see Figure S1). Thus, alkaline solutions of NO_3^- or NO_2^- (*ii, iii, iv* and *v*, respectively), were used to study the influence of dissolved O_2 and the impact of individual cations in solution. In addition to this, the amount Na^+ initially present in the NO_3^- and NO_2^- salts ($NaNO_3$ and $NaNO_2$) was minimized to individually address the impact of other alkali cations in solution different than Na^+. Then, the molar ratio of cations in solutions *(iv)* and *(v)* coming from the hydroxide is 14-fold larger than those coming from the NO_3^- or NO_2^- source salt. Samples were collected and analyzed for aqueous nitrogen species and pH all along the electrolysis. Experiments were performed in duplicate and deviations between them were lower than 5% for all trials.

2.3 Reactor characterization

The Reynolds number (Re) helps predict flow patterns in different fluid flow situations by measuring the ratio of inertial and viscous forces. This parameter is determined in PFR following (Eq. 1) [51].

$$Re = \frac{\rho \, d_{hyd} \, u_{avg}}{\mu} \quad (1)$$

where, ρ corresponds to the density of the solution (kg m^{-3}), μ to the dynamic viscosity (Pa s), d_{hyd} to the equivalent hydraulic diameter of the flow path (m) and u_{avg} to the mean liquid cross-flow velocity. The d_{hyd} is a function of the breadth of the channel, which corresponds to 0.031 m in this case (B in Eq (2)) and the interelectrode distance in the cell, which corresponds to 0.004 m in this case (S in Eq. (2)).

$$d_{hyd} = \frac{4\,BS}{2(B+S)} \tag{2}$$

The u_{avg} is calculated using Eq. (3).

$$u_{avg} = \frac{Q}{\varepsilon\,BS} \tag{3}$$

where Q is the liquid volumetric flow rate ($m^3\ s^{-1}$), ε is the porosity of the volume between the electrodes (accounting for the presence of the mass transfer promoter), and the product BS corresponds to the cross-sectional area perpendicular to the mean velocity.

2.4 Analytical techniques

The pH of the solution before and after treatment was measured using a pH meter Mettler Toledo Five Easy. The concentration of nitrogenated species in solution (NO_3^-, NO_2^-, and NH_3) was spectrophotometrically analyzed over time by a UV-vis spectrophotometer model DR1900 (HACH) using commercially available colorimetric kits: LCK 339 (mg NO_3^--N L^{-1}), LCK 341 (mg NO_2^--N L^{-1}) and LCK 304 (mg NH_3-N L^{-1}). In some cases, if the NO_2^- concentration is higher than 2.0 mg L^{-1} might interfere in the spectrophotometric NO_3^- quantification and produce high-bias results. To solve this, 50 mg of sulfamic (amidosulfonic) acid (H_2NSO_3H) were added to 5.0 mL of sample before NO_3^- quantification to remove any NO_2^- interference by sequestration.

The conversion (*NC*) of the initial oxyanion pollutant (x = NO_3^- or NO_2^-) was calculated using Eq. (4).

$$NC_x(\%) = \frac{C_{x,0} - C_{x,t}}{C_{x,0}} \times 100 \tag{4}$$

where $C_{x,0}$ is the concentration of the oxyanion pollutant in mg x-N L^{-1} at time zero, and $C_{x,t}$ is the concentration of the oxyanion pollutant at time (t). Previous works that quantified N-gas species evolution

159 (i.e., N_2, NO, NO_2 or N_2O) demonstrated that in most cases all the obtained gas corresponded to N_2 [52,53].
160 The quantification of gaseous nitrogen (N_{gas}) species was determined from mass balances on aqueous
161 nitrogen species and assumed to be preferentially N_2. Some NH_3 volatilization might occur near or above
162 the pK_a of 9.25 for NH_4^+/NH_3 (this is the case of solutions *ii*, *iii*, *iv* and *v*), but the Henry's constant is not
163 very large and such losses from solution of NH_3 gas would be highly depending upon mixing or gas-purging
164 conditions. Figure S2 reports an electrolysis at 20 mA cm^{-2} using NH_3 as the model pollutant at pH 12,
165 which demonstrates that NH_3 volatilization is negligible in all experiments reported here. The selectivity
166 towards nitrite ($S_{NO_2^-}$), N_{gas} evolution ($S_{N_{gas}}$) and ammonia (S_{NH_3}) was calculated using Eq. (5).

$$S_y(\%) = \frac{C_y}{C_{x,0} - C_{x,t}} \times 100 \quad (5)$$

167 where C_y represents the concentration (mg N L^{-1}) of a species produced over time, y = NO_2^-, N_{gas} or NH_3.
168 Electrical energy per order (*EE/O*), was used as an engineering figure of merit to benchmark the electric
169 energy required to reduce the concentration of the model pollutant by one order of magnitude in a unit
170 volume calculated from Eq. (6) for batch recirculation operation mode despite using a plug-flow reactor.

$$EE/O(kWh\ m^{-3} order^{-1}) = \frac{E_{cell} I t}{V_s log(C_0/C_t)} \quad (6)$$

171 where E_{cell} is the average of the cell potential (V), I is current intensity (A), t is time (h), V_s is solution
172 volume treated (L), and C_0 and C_t are the initial and final concentration after one order of magnitude
173 reduction.
174

175 **3. Results and discussion**

176 *3.1 Effect of the residence time of the* NO_3^- *solution in a batch recirculating plug flow reactor (PFR)*

177 ERN in the PFR was evaluated at three different solution flow rates 4.2, 21 and 105 mL min^{-1}, which
178 correspond to Reynolds numbers Re= 5, Re= 25 and Re= 123, respectively. These Re are representative of
179 a laminar flow, but susceptible to being disrupted by the mass transfer promoter within the cell. The
180 different hydrodynamic conditions result in different residence times of the electroactive species within the

reactor being shorter for higher flow-rates [51,54]. Moreover, the frequency of the NO_3^- in contact with the cathode in a recirculating reactor is also impacted by the flow rate, being higher for higher flow-rates. Figure 2 shows that NO_3^- removal after 180 min of electrolysis at initial pH 5.85 attain statistically the same NO_3^- conversion of ca. 57% for flow rates of 4.2 mL min^{-1} and 21.0 mL min^{-1}, but slightly higher removal of 66% for 105 mL min^{-1}. These results indicate that the frequency of the NO_3^- in contact with the cathode is more relevant than the residence time of NO_3^- within the recirculating reactor. Moreover, E_{cell} is similar among the different flow rates tested ($E_{cell\ -\ 4.2\ mL\ min^{-1}}$= 4.6 V, $E_{cell\ -\ 21\ mL\ min^{-1}}$ = 4.5 V and $E_{cell\ -\ 105\ mL\ min^{-1}}$ = 4.4 V). Nevertheless, the product selectivity (*S*) values for N_{gas} and NH_3 for each experiment remained constant. Resulting in a predominant selectivity of 70 – 73% for N_{gas} over the 18 – 20% for NH_3. These results support the fact that Sn cathode was selected in the present work for exploring the shift in selectivity from N_2 to NH_3, since it is a model electrode material for N_{gas} production from ERN. The main product from ERN and the selectivity ratio as $S_{N_{gas}}/S_{NH_3}$ remain constant independently of the type of mass transfer and residence time within the reactor. EE/O presented similar values ~36 kWh m^{-3} $order^{-1}$ for the lower flow rate conditions. However, the increased removal percentage observed at 105 mL m^{-1} resulted in a slight decrease of 20% in the EE/O to 29 kWh m^{-3} $order^{-1}$. These results suggest that higher flow rates may contribute to enhance mass transport and conversion if the solution is recirculated.

3.2 On the impact of pH control and dissolved O_2

During ERN at the cathode, there is the concomitant formation of hydroxyl anions at a high rate following Reactions (7) and (8) [55,56], which drastically change the pH at the proximity of the electrode and in the bulk. Figure S1 illustrates the fast pH change from neutral to alkaline (ca. 10.0) in only 5 min. A final pH value of 11.2 is reached at the end of 180 min electrolysis treatment. This pH increase is a commonly observed feature in unbuffered treated solutions, independently of the electrode material [57].

$$NO_3^- + 3\ H_2O + 5\ e^- \rightarrow 1/2N_{2(gas)} + 6\ OH^- \qquad E°= 0.25\ V\ vs\ SHE \qquad (7)$$

$$NO_3^- + 6\ H_2O + 8\ e^- \rightarrow NH_3 + 9\ OH^- \qquad E°= -0.12\ V\ vs\ SHE \qquad (8)$$

For this reason, an electrolysis for ERN at 21 mL min^{-1} and starting from an initial pH 12 solution (through base addition, i.e., NaOH) was performed to infer the pH effect (Fig. 2). At this initial pH, the electrolysis was pH-controlled since this initial value barely fluctuated over electrolysis time (see Figure S1). Sodium hydroxide is a common base used to rise pH during treatment and it was selected given its inert character as electrolyte in the electrochemical system. The pH-controlled electrolysis shown in Fig. 2 led to a NO_3^- conversion of 59%, with *S* values for N_{gas} of 71% and NH_3 of 20%, and EE/O of 31 kWh m^{-3} $order^{-1}$. These results at pH 12 are not significantly different from the performance of the electrolysis using a solution at an initial pH 6 under the same experimental conditions ([NO_3^--N] conversion = 57%, S_{N_2} = 73%, S_{NH_3} = 19% and EE/O = 36 kWh m^{-3} $order^{-1}$), according to a statistical two -sample *t*-test analysis based on obtained *p*-value of 0.206. These results imply a negligible impact of alkaline pH control on the overall ERN activity, selectivity, and the corresponding figures of merit. Thus, experiments were conducted at pH 12.0 from this point on.

The presence of dissolved oxygen gas in solution (≈ 0.26 mM) [58,59] represents a relevant factor to study, since could interfere in the ERN performance due to the concomitant oxygen reduction reaction (ORR). The ORR under acidic conditions can lead to the production of H_2O (Reaction (9)) and/or H_2O_2 (Reaction (10)). Whereas, under alkaline pH the formation of OH^- (Reaction (11)) and HO_2^- (Reaction (12)) products from ORR are favored [60–63]. A continuous flow of an inert gas within the treated solution has been suggested to eliminate any contribution from ORR to the global reduction process [56]. Thus, to evaluate the effect of dissolved O_2 on the performance of ERN, solutions were deaereated with argon (Ar) gas. Then, the bubbling of Ar was maintained thereafter during the entire electrolytic treatment. According to Fig. 2, the trial at 21 mL min^{-1} bubbling Ar in a solution at pH 12, led to [NO_3^--N] conversion = 63%, S_{N_2} = 74%, S_{NH_3} = 19% and EE/O = 30 kWh m^{-3} $order^{-1}$. Although the statistical two-sample *t*-test analysis shows a significant difference for NO_3^- removal based on obtained *p*-value of 0.002 between this experiment and the one in the presence of dissolved oxygen gas in solution, the difference among those values remains within the experimental error. Thus, these results may indicate that the presence of a very low concentration

of dissolved oxygen coming from air does not inhibit or significantly compete with the ERN. Therefore, it is concluded that the slight increase on NO_3^- removal attained by removing O_2 during ERN electrolysis is not justified given the increased complexity that large scale systems will face to remove dissolved oxygen during treatment.

$$O_2 + 4\,H^+ + 4\,e^- \rightarrow 2H_2O \qquad E°=1.23\ V\ vs\ SHE \qquad (9)$$

$$O_2 + 2\,H^+ + 2\,e^- \rightarrow H_2O_2 \qquad E°=0.70\ V\ vs\ SHE \qquad (10)$$

$$O_2 + 2\,H_2O + 4\,e^- \rightarrow 4\,OH^- \qquad E°=0.40\ V\ vs\ SHE \qquad (11)$$

$$O_2 + H_2O + 2\,e^- \rightarrow HO_2^- + OH^- \qquad E°=-0.065\ V\ vs\ SHE \qquad (12)$$

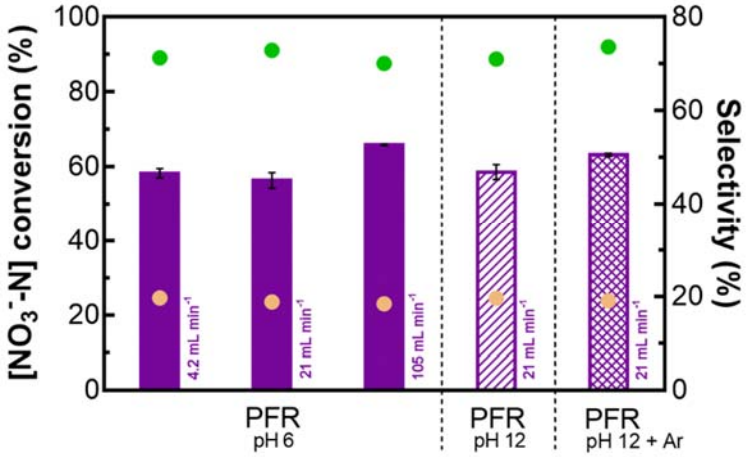

Figure 2. Nitrate conversion (bars) and selectivity towards N_{gas} (●) and NH_3 (●) obtained for the treatment of 100 mg NO_3^--N L^{-1} at 20 mA cm^{-2} and initial pH 6 or pH 12, with and without argon (Ar) bubbling, after 180 min, using a batch recirculation plug flow reactor (PFR) reactor at 4.2 mL min^{-1}, 21 mL min^{-1} and 105 mL min^{-1}, respectively.

3.3 Effect of alkali metal cations at the electrode-electrolyte interface during ERN

The effect of the supporting electrolyte containing different alkali cations such as lithium (Li^+), sodium (Na^+), potassium (K^+), and cesium (Cs^+) in low ionic strength pH 12 solutions on the ERN performance on Sn cathode is evaluated in this subsection. In particular, low ionic strength solutions are selected for

minimizing the presence of the counter cation from the nitrate source, as well as to mimic nitrate content in contaminated natural effluents [64]. These alkali species are susceptible to forming ionic pairs with negatively charged NO_3^- affecting its transport towards the negatively charged cathodic surface. Only monovalent alkali cations are studied here because it was demonstrated in a previous work [55] that divalent cations such as calcium (Ca^{2+}) and magnesium (Mg^{2+}) contribute to the scaling formation at the electrode surface. Figure 3a presents the evolution of N-species (mg-N L^{-1}) after 180 min of electrolysis for ERN. As can be observed, the NO_3^- concentration decreases from its initial value of 20.0 mg NO_3^--N L^{-1}, regardless of the supporting electrolyte used. However, the final NO_3^- concentrations were clearly affected by the nature of the cation present in solution. The NO_3^- conversion (and pseudo-first order kinetic constants) in each case were: 25% (k_1=2.7×10^{-5} s^{-1}), 41% (k_1=5.0×10^{-5} s^{-1}), 44% (k_1=5.3×10^{-5} s^{-1}) and 47% (k_1=5.9×10^{-5} s^{-1}) using LiOH, KOH, NaOH and CsOH, respectively. Table 1 summarizes key parameters such as the NO_3^- conversion and the selectivity towards NO_2^-, N_{gas}, and NH_3 for each electrolyte.

Thus, NO_3^- conversion is hardly impacted by the presence of Li^+ in solution. However, the presence of Na^+, K^+ or Cs^+ at low concentration display a minor effect on NO_3^- removal, which contrasts with some previous results reported for ERN in high ionic strength solutions [40]. Notably, product selectivity was severely impacted by the nature of the monovalent cation in solution as shown in Figure 3b and Table 1. The first alkali metal of the group (Li^+) favors the accumulation of NO_2^- and hinders further reduction to the final products. Nitrite reaches the highest concentration of 3.3 mg NO_2^--N L^{-1} with $S_{NO_2^-}$ = 65% resulting in a poor selectivity ratio for N_{gas} ($S_{N_{gas}}/S_{NO_2^-}$ = 0.3). In contrast, more bulky cations such as Cs^+ at the end of the alkali group increases the product selectivity for NH_3 generation (3.6 mg NH_3-N L^{-1} and S_{NH_3} = 39%), together with a more favorable product selectivity ratio for NH_3 ($S_{N_{gas}}/S_{NH_3}$= 1.3). The higher selectivity towards NH_3 for Sn electrocatalyst is a stark contrast to the usual reported values in literature generally < 20 % for Na^+ containing electrolytes, in which N_{gas} evolution was always the main product formed from ERN [15,65]. These differences suggest that electrolyte engineering may impact kinetics and selectivity based on the transport of not only NO_3^- but the ionic pair NO_3^--monovalent cation, which depending on

their affinity may affect coverage of N-species on the interface. Note that larger N-coverage might be required to favor the evolution for N_{gas} by the required formation of N≡N bonds during the cathodic reduction. Bulky cations such as Cs^+ may decrease N-coverage steering selectivity towards formation of NH_3. Despite N_{gas} remain as the main formed product from ERN in the presence of either NaOH, KOH and CsOH; the S_{NH_3} increases by 2.6-fold when transitioning from LiOH to CsOH (from 15% to 39%). Moreover, Table 1 shows a very different accumulation of NO_2^- in solution as a function of the alkali cation in the electrolyte, from $S_{NO_2^-}$ = 65% in presence of Li^+ to $S_{NO_2^-}$ = 13% in presence of Cs^+, which might be due to additional ionic pairs formed between NO_2^- and monovalent cations in solution. To understand more deeply this selectivity shift observed on ERN by varying the cation present in the electrode-electrolyte interface, additional electrolysis starting from nitrite (20.0 mg NO_2^--N L^{-1}) as the model pollutant in the presence of different electrolytes containing Li^+, Na^+, K^+ and Cs^+ in low ionic strength pH 12 solutions on a Sn cathode were also performed.

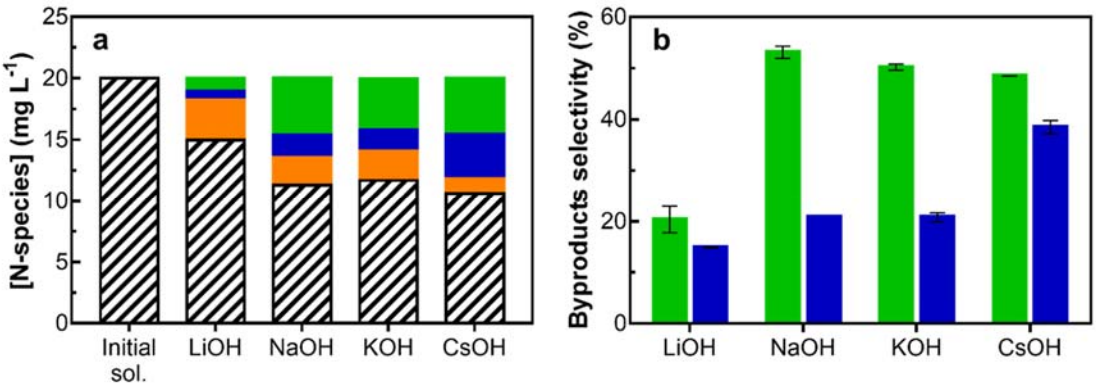

Figure 3. (a) Concentration of N-species (▨ NO_3^--N, ■ NO_2^--N, ■ NH_3-N, ■ N_{gas}-N) and (b) selectivity towards N_{gas} (■) and NH_3 (■) for the electrolysis of 20 mg NO_3^--N L^{-1} at 20 mA cm^{-2} after 180 min, using 0.02 M of different supporting electrolytes (LiOH, NaOH, KOH and CsOH) at pH 12 in a PFR.

Table 1. Key fitted and calculated parameters from the electroreduction of 20 mg NO_3^--N L^{-1} or 20 mg NO_2^--N L^{-1} in different electrolytes at 20 mA cm^{-2} and 180 min of treatment time.

Pollutant	Electrolyte	E_{cell} (V)	Pollutant conversion (%)	$k_1 \times 10^{-5}$ (s^{-1})	$S_{NO_2^-}$ (%)	$S_{NO_3^-}$ (%)	S_{Ngas} (%)	S_{NH_3} (%)
Nitrate	LiOH	5.9 ± 0.2	25 ± 1	2.7 ± 0.1	65 ± 1	-	20 ± 3	15 ± 1
	NaOH	5.9 ± 0.2	44 ± 1	5.3 ± 0.1	26 ± 1	-	53 ± 1	21 ± 1
	KOH	5.9 ± 0.1	41 ± 1	5.0 ± 0.1	29 ± 1	-	50 ± 1	21 ± 1
	CsOH	5.6 ± 0.2	47 ± 2	5.9 ± 0.4	13 ± 1	-	49 ± 1	39 ±1
Nitrite	LiOH	6.0 ± 0.1	36 ± 3	4.2 ± 0.5	-	61 ± 4	25 ± 1	14 ± 2
	NaOH	5.9 ± 0.1	52 ± 1	6.8 ± 0.1	-	33 ± 1	49 ± 1	18 ± 1
	KOH	6.0 ± 0.1	54 ± 2	7.2 ± 0.3	-	39 ± 2	44 ± 1	18 ± 1
	CsOH	5.6 ± 0.1	58 ± 1	8.1 ± 0.1	-	29 ± 1	36 ± 4	36 ± 4

3.4 Effect of alkali metal cations at the electrode-electrolyte interface during NO_2^- reduction

Figure 4a shows that the reduction of nitrite (20.0 mg NO_2^--N L^{-1}) follows a very similar trend to that obtained for NO_3^- removal (Figure 3a). After 180 min of treatment, the LiOH electrolyte remains the medium with the lowest pollutant conversion (36%), whereas the CsOH medium led to the highest NO_2^- removal (58%). The intermediate positions were relegated to NaOH and KOH, with 52% and 55%, respectively. The final concentrations of NO_2^- (and pseudo-first order kinetic constants) were: 12.4 mg NO_2^--N L^{-1} (k_1=4.2×10^{-5} s^{-1}), 9.7 mg NO_2^--N L^{-1} (k_1=6.8×10^{-5} s^{-1}), 9.0 mg NO_2^--N L^{-1} (k_1=7.2×10^{-5} s^{-1}) and 8.4 mg NO_2^--N L^{-1} (k_1=8.1×10^{-5} s^{-1}) for LiOH, NaOH, KOH and CsOH, respectively. Note that despite generally being the reduction of NO_3^- to NO_2^- considered the rate-limiting step, NO_2^- reduction can be also considered a sluggish reaction.

Evaluation of selectivity can be assessed from the NO_2^- reduction products as depicted in Figure 4b. Ammonia and nitrogen gas showing concentrations ranged from 1.0 to 4.4 mg NH_3-N L^{-1} and from 1.9 to 4.9 mg N_{gas}-N L^{-1}, respectively. However, there was observed some degree of NO_2^- oxidation yielding NO_3^- [66,67]. At the end of the electrolysis, the concentration of NO_3^- accumulated decreased from 4.4 mg NO_3^-

303 -N L^{-1} for Li^+ down to ca. 3.4 mg NO_3^--N L^{-1} for Cs^+. This result reinforces the hypothesis of the enhanced
304 mass transport of NO_2^- to the cathode aided by the formation of different ionic pairs depending on the alkali
305 metal present in solution, which would result in a decrease on competitive NO_2^- oxidation at the anode and
306 affects product selectivity. In fact, using LiOH as electrolyte induces by-product NO_3^- to become the main
307 product formed by exhibiting the highest selectivity ($S_{NO_3^-}$ = 61%) due to the blockage of N_{gas} and NH_3
308 production from NO_2^- reduction (see Table 1). In contrast, using NaOH or KOH as electrolyte, N_{gas} becomes
309 the main product detected (S_{Ngas} = 49% and 44%, respectively). Meanwhile, CsOH steers again selectivity
310 towards NH_3 generation (S_{NH_3} = 36%), which is equivalent to the one reported for N_{gas} (S_{Ngas}/S_{NH3} = 1.0).
311 Finally, Table 1 also allows to compare the S_{NH_3} obtained for the NO_3^- and the NO_2^- reduction reactions for
312 the case of all 4 different cations present in the electrode-electrolyte interface and surprisingly almost
313 identical values are reached in both reactions.
314 The electrolyte ions effect on the performance of different electrochemical systems has been already
315 reported for other electrochemical reactions, such as for instance on the electrohydrodimerization of
316 acrylonitrile to adiponitrile [68], being electrolyte ions determinant on the reaction rate and selectivity.
317 However, this effect was not evidenced before for NO_3^- and NO_2^- reduction reactions on Sn-based
318 electrodes. Thus, we present the first evidence proving that a significant shift in products selectivity from
319 N_{gas} towards either NO_2^- or NH_3 on Sn electrode can be achieved by properly tuning the electrode-
320 electrolyte interface through alkali cations. In fact, as reported by some authors, the size of alkali cations
321 influences the surface charge density at the electrode, availability of water molecules, and stability of
322 reaction intermediates [69–73]. A key element of the complex process of the NO_3^-/NO_2^- ion reduction path
323 on the surface of the Sn cathode at alkaline pH can be the adsorption of the nitrogen species [74]. Clearly,
324 adsorption takes place in the presence of the alkali cations, since these cations are located at the electrode-
325 electrolyte interface interacting with the negatively polarized cathode surface. The literature has
326 demonstrated that the generated electrical-field-surface-modified Sn, is determined by the atomic radius of
327 the cations: Li^+ (1.52 Å) < Na^+ (1.86 Å) < K^+ (2.31 Å) < Cs (2.62 Å) [75]. Moreover, other studies have

328 suggested that the primary role of cations at the electrode-electrolyte interface is to act as a promoter,
329 stabilizing negatively charged reaction intermediates by favorable electrostatic interactions via a local
330 electric field effect, as has been proposed for the case of the electrochemical reduction of CO_2 [76]. Thus,
331 we propose that a more powerful local electrostatic field is generated by solvated Cs^+ cations at the
332 electrode-electrolyte interface than by Li^+, Na^+ and K^+ cations, which allow a stronger stabilization of
333 reaction intermediates via molecule dipole - cation interactions during both NO_3^- and NO_2^- reduction
334 reactions. However, the symmetrical trigonal geometry displayed by NO_3^- gives as a result a zero net dipole
335 moment, which makes NO_3^- insensitive to the dipole – cation interactions. In contrast, NO_2^- presents a net
336 dipole moment and is sensitive to the local electric field generated by the species in solution. This fact could
337 justify the very close proximity between the results displayed in Figs. 3 and 4 (summarized in Table 1),
338 where NO_3^- removal as a function of the cations present in solution mimics the NO_2^- removal trend and
339 exhibits an increase in NH_3 production in the following order $Li^+ < Na^+ \approx K^+ < Cs^+$. Additionally, other
340 negatively charged intermediates formed during the reduction of NO_3^- and NO_2^- on Sn cathode, such as the
341 NO^- proposed by Katsounaros et al. (2012) [77], could also be favored by the stabilization provided by the
342 local electric field generated by different cations at the electrode-electrolyte interface.
343

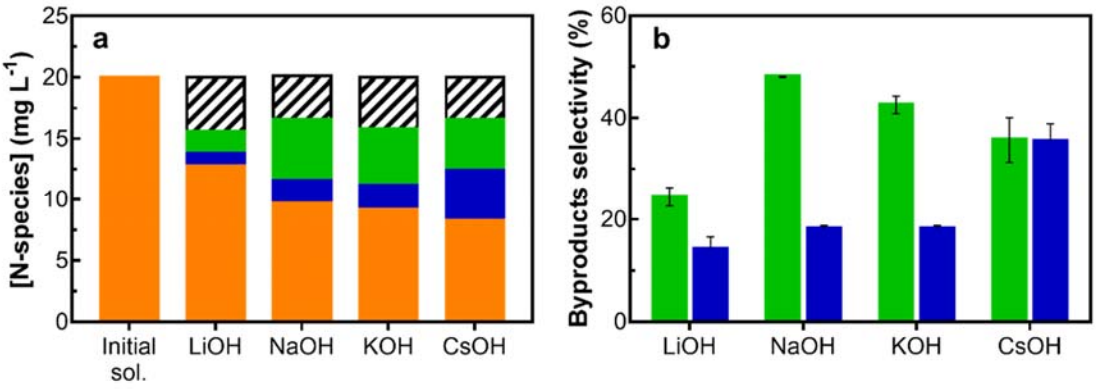

Figure 4. (a) Concentration of N-species (▨ NO_3^--N, ■ NO_2^--N, ■ NH_3-N, ■ N_{gas}-N) and (b) selectivity towards N_{gas} and NH_3 for the electrolysis of 20 mg NO_2^--N L^{-1} at 20 mA cm^{-2} after 180 min, using 0.02 M of different supporting electrolytes (LiOH, NaOH, KOH and CsOH) at pH 12 in a PFR.

3.5 Electrical energy per order considerations

Controlling electrode-electrolyte interfaces can become a prominent strategy not only to improve the reaction selectivity in electrochemical reactions and energy efficiency, but to minimize overall process costs. In Figure 5 is depicted the EE/O for the experiments related to the study of the effect of the alkali metal electrolytes on the reduction of NO_3^- and NO_2^- in low ionic strength alkaline solutions. For the case of NO_3^- removal (Fig. 5a), the EE/O ranged between 62 and 138 kWh m^{-3} $order^{-1}$. While for the case of NO_2^- removal (Fig. 5b), the same parameter ranged between 43 and 92 kWh m^{-3} $order^{-1}$. For both pollutants (i.e., NO_3^- and NO_2^-), the EE/O followed a similar trend where Li^+ led to the highest values and Cs^+ to the lowest. The determination of EE/O (Eq. (6)) depends on two main factors: cell potential (E_{cell}, Table 1) and the pollutant reduction kinetics rate (k_1, Fig. 5). As it can be seen in Table 1, E_{cell} is pratically the same for all the experiments (ca. 5.9 V), except for those using CsOH as electrolyte where is a bit smaller (5.6 V). However, k_1 is the factor that has more weight, as shown in Fig. 5 (red dots). For example, higher k_1 results in lower EE/O as is the case of Cs^+ and the contrary situation for Li^+ (lower higher k_1 leads to higher lower

EE/O). Therfore, electrode-electrolyte interface engineering can strongly modulate product selectivity as well as impact on reduction kinetics for both NO_3^- and NO_2^- reduction reactions.

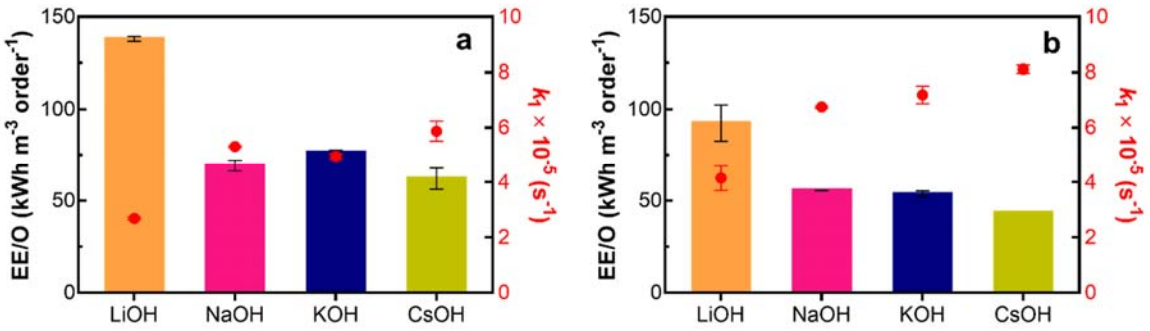

Figure 5. Electrical energy per order (bars) and pseudo-first order kinetics (red dots) for the electrolysis of (a) 20 mg NO_3^--N L^{-1} and (b) 20 mg NO_2^--N L^{-1} using 0.02 M of different supporting electrolytes (**LiOH**, **NaOH**, **KOH** and **CsOH**) at 20 mA cm^{-2} and pH 12 after 180 min in a PFR. Error bars do not exceed 5% of error.

4. Conclusions

In this work, the ERN performance at constant current on Sn electrode has been studied in a commercially available single compartment PFR, at natural or alkaline pH and in the presence of dissolved O_2 in solution, since it was demonstrated here that ORR does not significantly affect the performance of ERN. The aim of this work was to understand how solution composition, and particularly the electrolyte cation at the electrode-electrolyte interface, impacts on pollutants (NO_3^- and NO_2^-) removal rate and product selectivity in a membrane-less PFR. It is demonstrated the relevant effect of individual monovalent alkali cations in solution (Li^+, Na^+, K^+ and Cs^+), which control the main product formed, and modulate the selectivity in both NO_2^- and NO_3^- electrochemical reductions, as well as impact on the pollutant removal rate. In particular, it is reported for the first time a significant shift in ERN products selectivity from N_{gas} towards either NO_2^- or NH_3 production on a Sn cathode, which is a well-established highly active catalyst for N_{gas} and poor catalyst for NH_3 and NO_2^- production. Thus, tuning the electrode-electrolyte interface through the

electrolyte in solution represents a powerful tool for directing products selectivity and diminishing the treatment's process cost (from Li^+ to Cs^+). An unprecedented and significant impact of Cs^+ in solution for enhancing NH_3 selectivity in both NO_3^- and NO_2^- reduction reactions on Sn cathode was demonstrated. We suggest that NO_2^- reduction reaction controls products selectivity during ERN because the exact same trends were exhibited in both reactions. Additionally, Cs^+ in solution led to the lowest EE/O values with 62 kWh m^{-3} $order^{-1}$ and 43 kWh m^{-3} $order^{-1}$ for the NO_3^- and NO_2^- removal experiments, respectively. These values are 2-fold lower than compared with the same assays using Li^+. The relevant impact of Cs^+ is explained in terms of a higher strength of the local electric field generated at the electrode-electrolyte interface in comparison with the other cations evaluated, which stabilize intermediate products via molecule dipole - cation interactions. Thus, we propose modifying the main cation present in solution as a new tool to modulate ERN product selectivity different from the conventional catalyst engineering approach. Nevertheless, adding Cs^+ ions in solution to enhance NH_3 production from ERN is not intended nor applicable. The understanding of the impact of electrode/electrolyte impact on selective and kinetics may contribute to understand better significant shifts on product selectivity in different water matrices. For example, nuclear streams may contain high concentrations of NO_3^- and Cs^+ ions. Enhanced selectivity based on the electrode/electrolyte interface can be strategically used to benefit NH_3 production as well, which in combination with highly active catalysts for NH_3 generation from the ERN, could make feasible a more cost-efficient process than the Haber Bosh.

Acknowledgements

The authors acknowledge the support of the Centre National de la Recherche Scientifique (CNRS). This project has received funding from the European Union's Horizon 2020 research and innovation program under the Marie Sklodowska-Curie grant agreement No 843870. This material is based upon research supported by the Transatlantic Research Partnership of the Embassy of France in the United States and the FACE Foundation. This work has been partially funded by the CNRS Energy unit (Cellule Energie) through the project PEPS.

CRediT authorship contribution statement

Ana S. Fajardo: Methodology, Investigation, Data curation, Formal analysis, Validation, Visualization, Writing - original draft, Writing - review & editing. **Paul Westerhoff**: Project administration, Methodology, Formal analysis, Writing - review & editing. **Sergi Garcia-Segura**: Project administration, Data curation, Validation, Formal analysis, Writing - review & editing. **Carlos. M. Sánchez-Sánchez**: Supervision, Project administration, Conceptualization, Methodology, Data curation, Validation, Formal analysis, Writing - original draft, Writing - review & editing.

References

[1] WHO, Nitrate and nitrite in drinking-water, 2016. https://www.who.int/water_sanitation_health/dwq/chemicals/nitrate-nitrite-background-jan17.pdf?ua=1.

[2] EPA, National primary drinking water regulations, 2017. https://www.epa.gov/ground-water-and-drinking-water/national-primary-drinking-water-regulations.

[3] M.H. Ward, R.R. Jones, J.D. Brender, T.M. de Kok, P.J. Weyer, B.T. Nolan, C.M. Villanueva, S.G. van Breda, Drinking water nitrate and human health: An updated review, Int J Environ Res Public Health. 15 (2018) 1–31. https://doi.org/10.3390/ijerph15071557.

[4] R.R. Jones, P.J. Weyer, C.T. Dellavalle, M. Inoue-Choi, K.E. Anderson, K.P. Cantor, S. Krasner, K. Robien, L.E. Beane Freeman, D.T. Silverman, M.H. Ward, Nitrate from drinking water and diet and bladder cancer among postmenopausal women in Iowa, Environ Health Perspect. 124 (2016) 1751–1758. https://doi.org/10.1289/EHP191.

[5] A. Temkin, S. Evans, T. Manidis, C. Campbell, O. V. Naidenko, Exposure-based assessment and economic valuation of adverse birth outcomes and cancer risk due to nitrate in United States drinking water., Environ Res. 176 (2019) 108442. https://doi.org/10.1016/j.envres.2019.04.009.

[6] J. Schullehner, B. Hansen, M. Thygesen, C.B. Pedersen, T. Sigsgaard, Nitrate in drinking water and colorectal cancer risk: A nationwide population-based cohort study, Int J Cancer. 143 (2018) 73–79. https://doi.org/10.1002/ijc.31306.

[7] A.H. Wolfe, J.A. Patz, Reactive nitrogen and human health: Acute and long-term implications, Ambio. 31 (2002) 120–125. https://doi.org/10.1579/0044-7447-31.2.120.

[8] M.J. Pennino, J.E. Compton, S.G. Leibowitz, Trends in Drinking Water Nitrate Violations Across the United States, Environ Sci Technol. 51 (2017) 13450–13460. https://doi.org/10.1021/acs.est.7b04269.

[9] Y. Ren, Y. Ye, J. Zhu, K. Hu, Y. Wang, Characterization and evaluation of a macroporous anion exchange resin for nitrate removal from drinking water, Desalination Water Treat. 57 (2016) 17430–17439. https://doi.org/10.1080/19443994.2015.1085450.

[10] EPA, Nitrate removal from water supplies by ion exchange, 1978. https://nepis.epa.gov/Exe/ZyNET.exe/9102065Y.TXT?ZyActionD=ZyDocument&Client=EPA&Index=1976+Thru+1980&Docs=&Query=&Time=&EndTime=&SearchMethod=1&TocRestrict=n&Toc=&TocEntry=&QField=&QFieldYear=&QFieldMonth=&QFieldDay=&IntQFieldOp=0&ExtQFieldOp=0&XmlQuery=.

[11] A. Breytus, D. Hasson, R. Semiat, H. Shemer, Removal of nitrate from groundwater by Donnan dialysis, Journal of Water Process Engineering. 34 (2020) 101157. https://doi.org/10.1016/j.jwpe.2020.101157.

[12] J.W. Palko, D.I. Oyarzun, B. Ha, M. Stadermann, J.G. Santiago, Nitrate removal from water using electrostatic regeneration of functionalized adsorbent, Chemical Engineering Journal. 334 (2018) 1289–1296. https://doi.org/10.1016/j.cej.2017.10.161.

[13] V.B. Jensen, J.L. Darby, C. Seidel, C. Gorman, Nitrate in potable water supplies: Alternative management strategies, Crit Rev Environ Sci Technol. 44 (2014) 2203–2286. https://doi.org/10.1080/10643389.2013.828272.

[14] A.J. dos Santos, H.L. Barazorda-Ccahuana, G. Caballero-Manrique, Y. Chérémond, P.J. Espinoza-Montero, J.R. González-Rodríguez, U.J. Jáuregui-Haza, M.R.V. Lanza, A. Nájera, C. Oporto, A. Pérez Parada, T. Pérez, V.D. Quezada, V. Rojas, V. Sosa, A. Thiam, R.A. Torres-Palma, R. Vargas, S. Garcia-Segura, Accelerating innovative water treatment in Latin America, Nat Sustain. (2023). https://doi.org/10.1038/s41893-022-01042-z.

[15] A.S. Fajardo, P. Westerhoff, C.M. Sanchez-Sanchez, S. Garcia-Segura, Earth-abundant elements a sustainable solution for electrocatalytic reduction of nitrate, Appl Catal B. 281 (2021). https://doi.org/10.1016/j.apcatb.2020.119465.

[16] M. Li, C. Feng, Z. Zhang, N. Sugiura, Efficient electrochemical reduction of nitrate to nitrogen using Ti/IrO2-Pt anode and different cathodes, Electrochim Acta. 54 (2009) 4600–4606. https://doi.org/10.1016/j.electacta.2009.03.064.

[17] Z.A. Jonoush, A. Rezaee, A. Ghaffarinejad, Electrocatalytic nitrate reduction using Fe0/Fe3O4 nanoparticles immobilized on nickel foam: Selectivity and energy consumption studies, J Clean Prod. 242 (2020) 118569. https://doi.org/10.1016/j.jclepro.2019.118569.

[18] P. Kuang, K. Natsui, Y. Einaga, Comparison of performance between boron-doped diamond and copper electrodes for selective nitrogen gas formation by the electrochemical reduction of nitrate, Chemosphere. 210 (2018) 524–530. https://doi.org/10.1016/j.chemosphere.2018.07.039.

[19] Y. Zhang, Y. Zhao, Z. Chen, L. Wang, L. Zhou, P. Wu, F. Wang, P. Ou, Fe/Cu Composite Electrode Prepared by Electrodeposition and Its Excellent Behavior in Nitrate Electrochemical Removal, J Electrochem Soc. 165 (2018) E420–E428. https://doi.org/10.1149/2.0081810jes.

[20] Z. Shen, D. Liu, G. Peng, Y. Ma, J. Li, J. Shi, J. Peng, L. Ding, Electrocatalytic reduction of nitrate in water using Cu/Pd modified Ni foam cathode: High nitrate removal efficiency and N2-selectivity, Sep Purif Technol. 241 (2020). https://doi.org/10.1016/j.seppur.2020.116743.

[21] M. Marcos-Hernández, G. Antonio Cerrón-Calle, Y. Ge, S. Garcia-Segura, C.M. Sánchez-Sánchez, A.S. Fajardo, D. Villagrán, Effect of surface functionalization of Fe3O4 nano-enabled electrodes on the electrochemical reduction of nitrate, Sep Purif Technol. 282 (2022). https://doi.org/10.1016/j.seppur.2021.119771.

[22] P.H. van Langevelde, I. Katsounaros, M.T.M. Koper, Electrocatalytic Nitrate Reduction for Sustainable Ammonia Production, Joule. 5 (2021) 290–294. https://doi.org/10.1016/j.joule.2020.12.025.

[23] G.A. Cerrón-Calle, A.S. Fajardo, C.M. Sánchez-Sánchez, S. Garcia-Segura, Highly reactive Cu-Pt bimetallic 3D-electrocatalyst for selective nitrate reduction to ammonia, Appl Catal B. 302 (2022). https://doi.org/10.1016/j.apcatb.2021.120844.

[24] G.A. Cerrón-Calle, T.P. Senftle, S. Garcia-Segura, Strategic tailored design of electrocatalysts for environmental remediation based on density functional theory (DFT) and microkinetic modeling, Curr Opin Electrochem. 35 (2022). https://doi.org/10.1016/j.coelec.2022.101062.

[25] J. Lim, C.Y. Liu, J. Park, Y.H. Liu, T.P. Senftle, S.W. Lee, M.C. Hatzell, Structure Sensitivity of Pd Facets for Enhanced Electrochemical Nitrate Reduction to Ammonia, ACS Catal. 11 (2021) 7568–7577. https://doi.org/10.1021/acscatal.1c01413.

[26] Y. Liu, B. Deng, K. Li, H. Wang, Y. Sun, F. Dong, Metal-organic framework derived carbon-supported bimetallic copper-nickel alloy electrocatalysts for highly selective nitrate reduction to ammonia, J Colloid Interface Sci. 614 (2022) 405–414. https://doi.org/10.1016/j.jcis.2022.01.127.

[27] L. Mattarozzi, S. Cattarin, N. Comisso, P. Guerriero, M. Musiani, L. Vázquez-Gómez, E. Verlato, Electrochemical reduction of nitrate and nitrite in alkaline media at CuNi alloy electrodes, Electrochim Acta. 89 (2013) 488–496. https://doi.org/10.1016/j.electacta.2012.11.074.

[28] W. He, J. Zhang, S. Dieckhöfer, S. Varhade, A.C. Brix, A. Lielpetere, S. Seisel, J.R.C. Junqueira, W. Schuhmann, Splicing the active phases of copper/cobalt-based catalysts achieves high-rate tandem electroreduction of nitrate to ammonia, Nat Commun. 13 (2022). https://doi.org/10.1038/s41467-022-28728-4.

[29] G.A. Cerrón-Calle, A. Wines, S. Garcia-Segura, Atomic hydrogen provision by cobalt sites in a bimetallic Ni/Co(OH)x and trimetallic Ni/Cu2O/Co(OH)x configurations for superior ammonia production, Appl Catal B. 328 (2023). https://doi.org/10.1016/j.apcatb.2023.122540.

[30] J. Zhao, X. Ren, X. Liu, X. Kuang, H. Wang, C. Zhang, Q. Wei, D. Wu, Zn single atom on N-doped carbon: Highly active and selective catalyst for electrochemical reduction of nitrate to ammonia, Chemical Engineering Journal. 452 (2023). https://doi.org/10.1016/j.cej.2022.139533.

[31] Z.Y. Wu, M. Karamad, X. Yong, Q. Huang, D.A. Cullen, P. Zhu, C. Xia, Q. Xiao, M. Shakouri, F.Y. Chen, J.Y. (Timothy) Kim, Y. Xia, K. Heck, Y. Hu, M.S. Wong, Q. Li, I. Gates, S. Siahrostami, H. Wang, Electrochemical ammonia synthesis via nitrate reduction on Fe single atom catalyst, Nat Commun. 12 (2021). https://doi.org/10.1038/s41467-021-23115-x.

[32] A. Wu, Y. Zhou, J. Lv, D. Zhang, Y. Peng, Q. Ye, P. Fu, W. Wang, X. Lin, S. Liu, M. Xu, Z. Qi, S. Zhu, W. Zhu, J. Yan, X. Tu, X. Li, Boosting Electrocatalytic Nitrate-to-Ammonia Conversion via Plasma Enhanced CuCo Alloy-Substrate Interaction, ACS Sustain Chem Eng. 10 (2022) 14539–14548. https://doi.org/10.1021/acssuschemeng.2c04249.

[33] W. Fu, Y. Du, J. Jing, C. Fu, M. Zhou, Highly selective nitrate reduction to ammonia on CoO/Cu foam via constructing interfacial electric field to tune adsorption of reactants, Appl Catal B. 324 (2023). https://doi.org/10.1016/j.apcatb.2022.122201.

[34] C. Wang, Z. Liu, L. Dong, F. Du, J. Li, C. Chen, R. Ma, C. Li, C. Guo, Bimetallic CuCo nanocrystals to tailor absorption energy of intermediators for efficient electrochemical nitrate conversion to ammonia in neutral electrolyte, J Power Sources. 556 (2023). https://doi.org/10.1016/j.jpowsour.2022.232523.

[35] Z. Niu, S. Fan, X. Li, P. Wang, Z. Liu, J. Wang, C. Bai, D. Zhang, Bifunctional copper-cobalt spinel electrocatalysts for efficient tandem-like nitrate reduction to ammonia, Chemical Engineering Journal. 450 (2022). https://doi.org/10.1016/j.cej.2022.138343.

[36] G.A. Cerrón-Calle, A.S. Fajardo, J. Liu, C.M. Sánchez-Sánchez, S. Garcia-Segura, Enabling circular economy by N-recovery: Electrocatalytic reduction of nitrate with cobalt hydroxide nanocomposites on copper foam treating low conductivity groundwater effluents, Science of The Total Environment. 887 (2023) 163938. https://doi.org/10.1016/j.scitotenv.2023.163938.

[37] D. Li, W. Gao, C. Geng, J. Meng, Y. Guan, J. Liang, L. Zhang, Low-nitrite generation Cu–Co/Ti cathode materials for electrochemical nitrate reduction, Environmental Science and Pollution Research. 30 (2023) 18563–18576. https://doi.org/10.1007/s11356-022-23517-4.

[38] M.M. Waegele, C.M. Gunathunge, J. Li, X. Li, How cations affect the electric double layer and the rates and selectivity of electrocatalytic processes, Journal of Chemical Physics. 151 (2019) 1DUMMT. https://doi.org/10.1063/1.5124878.

[39] J.M. McEnaney, S.J. Blair, A.C. Nielander, J.A. Schwalbe, D.M. Koshy, M. Cargnello, T.F. Jaramillo, Electrolyte engineering for efficient electrochemical nitrate reduction to ammonia on a

titanium electrode, ACS Sustain Chem Eng. 8 (2020) 2672–2681. https://doi.org/10.1021/acssuschemeng.9b05983.

[40] I. Katsounaros, G. Kyriacou, Influence of the concentration and the nature of the supporting electrolyte on the electrochemical reduction of nitrate on tin cathode, Electrochim Acta. 52 (2007) 6412–6420. https://doi.org/10.1016/j.electacta.2007.04.050.

[41] I. Katsounaros, D. Ipsakis, C. Polatides, G. Kyriacou, Efficient electrochemical reduction of nitrate to nitrogen on tin cathode at very high cathodic potentials, Electrochim Acta. 52 (2006) 1329–1338. https://doi.org/10.1016/j.electacta.2006.07.034.

[42] M. Dortsiou, I. Katsounaros, C. Polatides, G. Kyriacou, Influence of the electrode and the pH on the rate and the product distribution of the electrochemical removal of nitrate, Environmental Technology (United Kingdom). 34 (2013) 373–381. https://doi.org/10.1080/09593330.2012.696722.

[43] S. Banerjee, X. Han, V.S. Thoi, Modulating the Electrode-Electrolyte Interface with Cationic Surfactants in Carbon Dioxide Reduction, ACS Catal. 9 (2019) 5631–5637. https://doi.org/10.1021/acscatal.9b00449.

[44] M. Moura de Salles Pupo, R. Kortlever, Electrolyte Effects on the Electrochemical Reduction of CO2, ChemPhysChem. 20 (2019) 2926–2935. https://doi.org/10.1002/cphc.201900680.

[45] S. Verma, X. Lu, S. Ma, R.I. Masel, P.J.A. Kenis, The effect of electrolyte composition on the electroreduction of CO2 to CO on Ag based gas diffusion electrodes, Physical Chemistry Chemical Physics. 18 (2016) 7075–7084. https://doi.org/10.1039/c5cp05665a.

[46] E. Vichou, A. Solé-Daura, C. Mellot-Draznieks, Y. Li, M. Gomez-Mingot, M. Fontecave, C.M. Sánchez- Sánchez, Electrocatalytic Conversion of CO2 to Formate at Low Overpotential by Electrolyte Engineering in Model Molecular Catalysis, ChemSusChem. (2022). https://doi.org/10.1002/cssc.202201566.

[47] J. Fu, F. Yao, T. Xie, Y. Zhong, Z. Tao, S. Chen, L. He, Z. Pi, K. Hou, D. Wang, X. Li, Q. Yang, In-situ growth of needle-like Co3O4 on cobalt foam as a self-supported cathode for electrochemical reduction of nitrate, Sep Purif Technol. 276 (2021). https://doi.org/10.1016/j.seppur.2021.119329.

[48] R. Oriol, M. del P. Bernícola, E. Brillas, P.L. Cabot, I. Sirés, Paired electro-oxidation of insecticide imidacloprid and electrodenitrification in simulated and real water matrices, Electrochim Acta. 317 (2019) 753–765. https://doi.org/10.1016/j.electacta.2019.05.002.

[49] J. Gao, B. Jiang, C. Ni, Y. Qi, Y. Zhang, N. Oturan, M.A. Oturan, Non-precious Co3O4-TiO2/Ti cathode based electrocatalytic nitrate reduction: Preparation, performance and mechanism, Appl Catal B. 254 (2019) 391–402. https://doi.org/10.1016/j.apcatb.2019.05.016.

[50] Y. Zhang, Y. Zhao, Z. Chen, L. Wang, P. Wu, F. Wang, Electrochemical reduction of nitrate via Cu/Ni composite cathode paired with Ir-Ru/Ti anode: High efficiency and N2 selectivity, Electrochim Acta. 291 (2018) 151–160. https://doi.org/10.1016/j.electacta.2018.08.154.

[51] W.S. Walker, E. Bezerra Cavalcanti, A. Atrashkevich, A.S. Fajardo, E. Brillas, S. Garcia-Segura, Mass transfer and residence time distribution in an electrochemical cell with an air-diffusion electrode: Effect of air pressure and mesh promoters, Electrochim Acta. 378 (2021). https://doi.org/10.1016/j.electacta.2021.138131.

[52] X. Chen, T. Zhang, M. Kan, D. Song, J. Jia, Y. Zhao, X. Qian, Binderless and Oxygen Vacancies Rich FeNi/Graphitized Mesoporous Carbon/Ni Foam for Electrocatalytic Reduction of Nitrate, Environ Sci Technol. 54 (2020) 13344–13353. https://doi.org/10.1021/acs.est.0c05631.

[53] W. Teng, N. Bai, Y. Liu, Y. Liu, J. Fan, W.X. Zhang, Selective Nitrate Reduction to Dinitrogen by Electrocatalysis on Nanoscale Iron Encapsulated in Mesoporous Carbon, Environ Sci Technol. 52 (2018) 230–236. https://doi.org/10.1021/acs.est.7b04775.

[54] A.S. Fajardo, R.C. Martins, D.R. Silva, C.A. Martínez-Huitle, R.M. Quinta-Ferreira, Dye wastewaters treatment using batch and recirculation flow electrocoagulation systems, Journal of Electroanalytical Chemistry. 801 (2017) 30–37. https://doi.org/10.1016/j.jelechem.2017.07.015.

[55] A. Atrashkevich, A.S. Fajardo, P. Westerhoff, W.S. Walker, C.M. Sánchez-Sánchez, S. Garcia-Segura, Overcoming barriers for nitrate electrochemical reduction: By-passing water hardness, Water Res. 225 (2022) 119118. https://doi.org/10.1016/j.watres.2022.119118.

[56] I. Katsounaros, On the assessment of electrocatalysts for nitrate reduction, Curr Opin Electrochem. 28 (2021) 100721. https://doi.org/10.1016/j.coelec.2021.100721.

[57] I. Katsounaros, J.C. Meier, S.O. Klemm, A.A. Topalov, P.U. Biedermann, M. Auinger, K.J.J. Mayrhofer, The effective surface pH during reactions at the solid-liquid interface, Electrochem Commun. 13 (2011) 634–637. https://doi.org/10.1016/j.elecom.2011.03.032.

[58] T. Kaskiala, Determination of oxygen solubility in aqueous sulphuric acid media q, n.d. www.elsevier.com/locate/mineng.

[59] R.N. Itoe, G.D. Wesson, E.E. Kalu, Evaluation of Oxygen Transport Parameters in H2SO4-CH3OH Mixtures Using Electrochemical Methods, J Electrochem Soc. 147 (2000) 2445. https://doi.org/10.1149/1.1393551.

[60] A. Prieto, J. Hernández, E. Herrero, J.M. Feliu, The role of anions in oxygen reduction in neutral and basic media on gold single-crystal electrodes, Journal of Solid State Electrochemistry. 7 (2003) 599–606. https://doi.org/10.1007/s10008-003-0362-3.

[61] B. Dembinska, K. Brzozowska, A. Szwed, K. Miecznikowski, E. Negro, V. Di Noto, P.J. Kulesza, Electrocatalytic Oxygen Reduction in Alkaline Medium at Graphene-Supported Silver-Iron Carbon Nitride Sites Generated During Thermal Decomposition of Silver Hexacyanoferrate, Electrocatalysis. 10 (2019) 112–124. https://doi.org/10.1007/s12678-018-0501-3.

[62] C.M. Sánchez-Sánchez, A.J. Bard, Hydrogen peroxide production in the oxygen reduction reaction at different electrocatalysts as quantified by scanning electrochemical microscopy, Anal Chem. 81 (2009) 8094–8100. https://doi.org/10.1021/ac901291v.

[63] E. Yeager, Electrocatalysts for O2 reduction, Electrochim Acta. 29 (1984) 1527–1537.

[64] S. Garcia-Segura, A.B. Nienhauser, A.S. Fajardo, R. Bansal, C.L. Coonrod, J.D. Fortner, M. Marcos-Hernández, T. Rogers, D. Villagran, M.S. Wong, P. Westerhoff, Disparities between

experimental and environmental conditions: Research steps toward making electrochemical water treatment a reality, Curr Opin Electrochem. 22 (2020) 9–16. https://doi.org/10.1016/j.coelec.2020.03.001.

[65] I. Katsounaros, M. Dortsiou, G. Kyriacou, Electrochemical reduction of nitrate and nitrite in simulated liquid nuclear wastes, J Hazard Mater. 171 (2009) 323–327. https://doi.org/10.1016/j.jhazmat.2009.06.005.

[66] K. Nakata, Y. Doi, S. Kubota, K. Shimazu, Reduction of nitrite on tin-modified noble metal electrodes, Journal of Electroanalytical Chemistry. 647 (2010) 187–193. https://doi.org/10.1016/j.jelechem.2010.06.003.

[67] Y. Wang, E. Laborda, R.G. Compton, Electrochemical oxidation of nitrite: Kinetic, mechanistic and analytical study by square wave voltammetry, Journal of Electroanalytical Chemistry. 670 (2012) 56–61. https://doi.org/10.1016/j.jelechem.2012.02.016.

[68] D.E. Blanco, R. Atwi, S. Sethuraman, A. Lasri, J. Morales, N.N. Rajput, M.A. Modestino, Effect of Electrolyte Cations on Organic Electrosynthesis: The Case of Adiponitrile Electrochemical Production, J Electrochem Soc. 167 (2020) 155526. https://doi.org/10.1149/1945-7111/abc766.

[69] M.R. Singh, Y. Kwon, Y. Lum, J.W. Ager, A.T. Bell, Hydrolysis of Electrolyte Cations Enhances the Electrochemical Reduction of CO2 over Ag and Cu, J Am Chem Soc. 138 (2016) 13006–13012. https://doi.org/10.1021/jacs.6b07612.

[70] L.D. Chen, M. Urushihara, K. Chan, J.K. Nørskov, Electric Field Effects in Electrochemical CO2 Reduction, ACS Catal. 6 (2016) 7133–7139. https://doi.org/10.1021/acscatal.6b02299.

[71] J. Resasco, L.D. Chen, E. Clark, C. Tsai, C. Hahn, T.F. Jaramillo, K. Chan, A.T. Bell, Promoter Effects of Alkali Metal Cations on the Electrochemical Reduction of Carbon Dioxide, J Am Chem Soc. 139 (2017) 11277–11287. https://doi.org/10.1021/jacs.7b06765.

[72] M.R. Thorson, K.I. Siil, P.J.A. Kenis, Effect of Cations on the Electrochemical Conversion of CO 2 to CO , J Electrochem Soc. 160 (2013) F69–F74. https://doi.org/10.1149/2.052301jes.

642 [73] A. Manzo-Robledo, C. Lévy-Clément, N. Alonso-Vante, The interplay between hydrogen evolution
643 reaction and nitrate reduction on boron-doped diamond in aqueous solution: The effect of alkali
644 cations, Electrochim Acta. 117 (2014) 420–425. https://doi.org/10.1016/j.electacta.2013.11.151.
645 [74] A. Manzo-Robledo, C. Lévy-Clément, N. Alonso-Vante, Electrochemical behavior of nitrogen gas
646 species adsorbed onto boron-doped diamond (BDD) electrodes, Langmuir. 23 (2007) 11413–11416.
647 https://doi.org/10.1021/la701875h.
648 [75] W.J. Xie, Z. Zhang, Y.Q. Gao, Ion Pairing in Alkali Nitrate Electrolyte Solutions, Journal of
649 Physical Chemistry B. 120 (2016) 2343–2351. https://doi.org/10.1021/acs.jpcb.5b10755.
650 [76] M.C.O. Monteiro, F. Dattila, B. Hagedoorn, R. García-Muelas, N. López, M.T.M. Koper, Absence
651 of CO2 electroreduction on copper, gold and silver electrodes without metal cations in solution, Nat
652 Catal. 4 (2021) 654–662. https://doi.org/10.1038/s41929-021-00655-5.
653 [77] I. Katsounaros, M. Dortsiou, C. Polatides, S. Preston, T. Kypraios, G. Kyriacou, Reaction pathways
654 in the electrochemical reduction of nitrate on tin, Electrochim Acta. 71 (2012) 270–276.
655 https://doi.org/10.1016/j.electacta.2012.03.154.
656

SUPPORTING INFORMATION

Selectivity modulation during electrochemical reduction of nitrate by electrolyte engineering

Ana S. Fajardo[a,b,*], Paul Westerhoff[b], Sergi Garcia-Segura[b] and Carlos M. Sánchez-Sánchez[a,**]

[a]Sorbonne Université, CNRS, Laboratoire Interfaces et Systèmes Electrochimiques (LISE), 4 place Jussieu, F-75005, Paris, France

[b]Nanosystems Engineering Research Center for Nanotechnology-Enabled Water Treatment, School of Sustainable Engineering and the Built Environment, Arizona State University, Tempe, AZ 85287-3005, USA

Corresponding author:

*e-mail: sofia.fajardo@ipc.pt (Dr. Ana Sofia Fajardo)

**e-mail: carlos.sanchez@sorbonne-universite.fr (Dr. Carlos M. Sanchez-Sanchez)

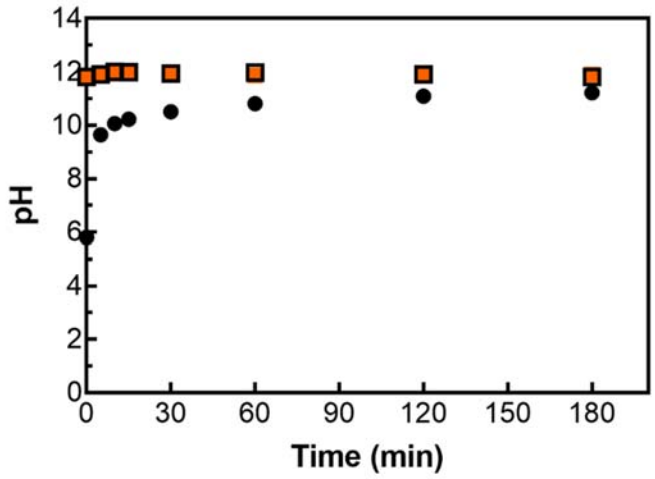

21

22 **Figure S1.** pH evolution over time during the pollutant electroreduction on Sn cathode in a plug flow

23 reactor at 20 mA cm^{-2} of 3 different solutions: (●) 100 mg L^{-1} NO_3^--N in 0.05 mol L^{-1} Na_2SO_4, (□) 20 mg

24 L^{-1} NO_3^--N in 0.02 mol L^{-1} NaOH and (■) 20 mg L^{-1} NO_2^--N in 0.02 mol L^{-1} NaOH.

25

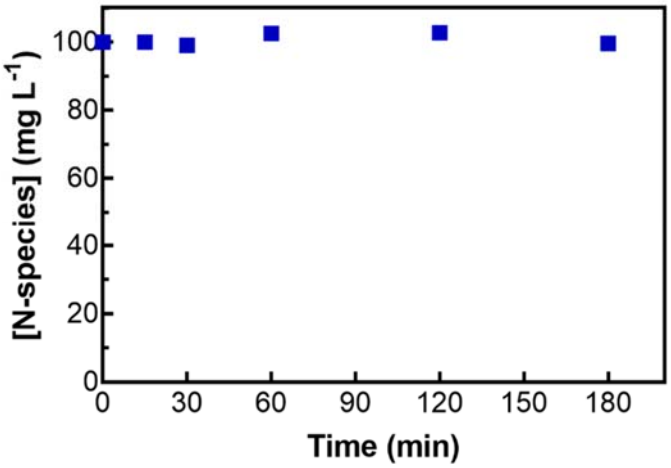

Figure S2. Evolution of the NH_3-N concentration over time during the electroreduction of 100 mg L^{-1} NH_3-N in 0.05 mol L^{-1} Na_2SO_4 and 0.01 mol L^{-1} NaOH (pH = 12) at 20 mA cm^{-2} using Sn as the cathode material in a plug flow reactor.